Electrochimica Acta 154 (2015) 468–475

Contents lists available at ScienceDirect

Electrochimica Acta

journal homepage: www.elsevier.com/locate/electacta

Comparison of the performance of flow-by three-dimensional cylindrical electrochemical reactors with inner or outer counter electrode under limiting current conditions

A.N. Colli, J.M. Bisang *

Programa de Electroquímica Aplicada e Ingeniería Electroquímica (PRELINE), Facultad de Ingeniería Química, Universidad Nacional del Litoral, Santiago del Estero 2829, S3000AOM Santa Fe, Argentina

ARTICLE INFO

Article history:
Received 22 September 2014
Received in revised form 20 November 2014
Accepted 12 December 2014
Available online 15 December 2014

Keywords:
electrochemical reactors
mass-transfer coefficient
metal removal
potential distribution
three-dimensional electrodes

ABSTRACT

The influence of the position of the counter electrode on the behaviour of a cylindrical electrochemical reactor with a three-dimensional electrode in flow-by configuration is analysed. Experimental results of the potential distribution are compared with theoretical predictions obtaining a close agreement between them. The best performance was observed for the arrangement with an outer counter electrode, where the largest bed thickness is obtained for a given potential difference in the three-dimensional structure; which, under limiting current conditions, tolerates a higher current increasing the conversion per pass. The reactor was also checked for the removal of copper from dilute solutions and the experimental results coincide with the theoretical predictions. The morphology of the electrodeposited copper is discussed as a function of the radial position inside the three-dimensional structure.

1. Introduction

Three-dimensional structures are required as electrodes to increase the space time yield of electrochemical reactors when the reactions take place at low current densities such as in the processing of contaminants from waste waters. These electrodes were recently reviewed [1] and a parallelepiped configuration is frequently preferred for the reactor. However, a cylindrical arrangement is necessary in some cases in the industrial practice. Thus, a pioneer cylindrical electrochemical reactor with a three-dimensional anode of lead pellets was used in the Nalco process for the production of lead alkyls [2]. Van der Heiden et al. [3,4] reported the removal of metals from dilute solutions by fluidised bed electrolysis using a cylindrical configuration with many anodic compartments made of a diaphragm with a central wire as anode, which are symmetrically placed in only one cathode. Around each diaphragm six bar-shaped contact feeders are installed to supply the fluidised bed with current. This type of cell construction presents a radial potential distribution around each anode. The Zadra-IMT process for the direct electrowinning of gold is based on a cylindrical three-dimensional cathode of steel wool [5].

The cylindrical configuration is also used in three-dimensional rotating electrodes. A rotating packed bed electrode [6] and a vertically moving particle bed electrode were proposed [7,8]. Reade et al. [9] studied the performance of a reticulated vitreous carbon rotating cylinder electrode, where an electrolyte jet impinged on the bottom central part of the electrode enhancing the mass-transfer coefficient. Likewise, the mass-transfer behaviour of rotating cylinder electrodes made of expanded metal sheets [10], woven wire meshes [11] and wedge wire screens [12] was also examined. Recently, a three-dimensional rotating electrode with a two phase flow induced by centrifugal force was studied for the production of alkaline peroxide by the electrochemical reduction of oxygen [13]. Alkire and Ng [14,15] proposed a mathematical model for cylindrical electrochemical reactors with a packed-bed of flow-by configuration.

In all these cases of cylindrical electrochemical reactors the outer or inner location of the counter electrode related to the three-dimensional structure is of crucial importance for the performance of the equipment [16], because in the cylindrical geometry, with current and electrolyte flow at a right angle, the cross-sectional area for the current flow in the solution phase depends on the radial position.

It is the purpose of the present contribution to analyse experimentally the potential distribution in a cylindrical geometry, either with outer or inner location of the counter electrode, in

* Corresponding author. Tel.: +54 342 4571164; fax.: +54 342 4571164
E-mail address: jbisang@fiq.unl.edu.ar (J.M. Bisang).

http://dx.doi.org/10.1016/j.electacta.2014.12.076
0013-4686/

order to find the best arrangement for an electrochemical reactor with a three-dimensional working electrode and to assess the accuracy of the continuous model for these equipments.

2. Mathematical modelling

Fig. 1 shows schematically a cylindrical electrochemical reactor with a three-dimensional electrode. Part (a) corresponds to the configuration with outer counter electrode and Part (b) to the inner case. In the following theoretical analysis, based on the continuous model of three-dimensional electrodes, some usual simplifying assumptions are made: (i) the void fraction and the surface area per unit electrode volume are uniform and do not change with time, (ii) the effective resistivity of the metal phase is negligible in comparison to that of the solution phase, (iii) the electrolyte velocity is constant across the cross-section of the reactor, (iv) a single electrode reaction takes place under limiting current conditions, and (v) the reactor is isothermal and in steady state. Additionally, the change in concentration inside the three-dimensional electrode was considered negligible, which represents a rough approximation allowing a simplification in the modelling. The current balance in the solution phase yields

$$\frac{dI_s(r)}{dr} = j(r)A_s 2\pi r h \tag{1}$$

where I_s is the current in the solution phase at the radial position r, A_s is the surface area per unit electrode volume and h is the electrode length. Assuming all points under limiting current conditions, the total current drained by the electrode, I_L, can be obtained by integration of Eq. (1)

$$I_L = j_L A_S \pi h (r_e^2 - r_i^2) \tag{2}$$

where r_e and r_i are the external and internal radius of the three-dimensional electrode, respectively and the limiting current density, j_L, is given by

$$j_L = \nu_e F k_m c \tag{3}$$

here ν_e is the number of electrons interchanged, F is the Faraday constant, k_m is the global mass-transfer coefficient and c is the bulk concentration. Introducing Eq. (2) into Eq. (1) and integrating is

$$I_s(r) = I_L \frac{r^2 - r_{ref}^2}{r_e^2 - r_i^2} \tag{4}$$

being $r_{ref} = r_i$ for the outer counter electrode case and $r_{ref} = r_e$ when the counter electrode is internal.

The Ohm's law for the solution phase is

$$\frac{d\varphi_s(r)}{dr} = -\rho \frac{I_s(r)}{2\pi r h} \tag{5}$$

where φ_s is the potential in the solution phase and ρ is the effective electrolyte resistivity, evaluated by the Bruggeman equation

$$\rho = \rho^0 \varepsilon^{-3/2} \tag{6}$$

being ρ^0 the electrolyte resistivity and ε the void fraction of the three-dimensional structure. Defining the local electrode potential, E, against any reference electrode as

$$E(r) = \varphi_m - \varphi_s(r) \tag{7}$$

here φ_m is the potential in the metal phase, which is assumed isopotential. Thus, the mathematical model is valid for cylindrical electrochemical reactors with a three-dimensional electrode made of meshes, expanded metal sheets, felts, foams, clothes or packed beds of conductive particles. Combining Eqs. (4), (5), and (7) yields

$$E(r) = E(r_i) + \frac{\rho I_L}{2\pi h (r_e^2 - r_i^2)} \int_{r_i}^{r} \left(r - \frac{r_{ref}^2}{r}\right) dr \tag{8}$$

The potential distribution inside the three-dimensional electrode is obtained by integration of Eq. (8)

$$E(r) = E(r_i) + \frac{\rho I_L}{2V} \left(\frac{r^2 - r_i^2}{2} - r_{ref}^2 \ln \frac{r}{r_i} \right) \tag{9}$$

being V the volume of the three-dimensional structure and I_L is negative for a cathodic process and positive for an anodic one. Evaluating Eq. (9) at the external radius and rearranging yields

$$\frac{E(r_e) - E(r_i)}{\rho I_L} = \frac{1}{2V} \left(\frac{r_e^2 - r_i^2}{2} - r_{ref}^2 \ln \frac{r_e}{r_i} \right) \tag{10}$$

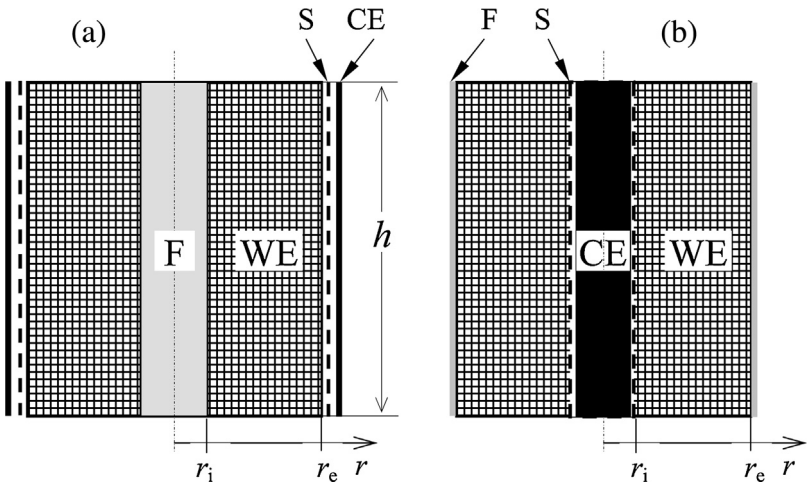

Fig. 1. Schematic view of the two arrangements of cylindrical electrochemical reactors with three-dimensional electrodes used in the mathematical model. (a) Outer counter electrode. (b) Inner counter electrode. CE: counter electrode, WE: three-dimensional electrode, F: current feeder, S: separator.

where the right hand side of Eq. (10) depends only on geometrical parameters of the three-dimensional structure. Appling Eq. (10) to the arrangements with outer and inner counter electrode, OCE and ICE respectively, and assuming the same potential difference at the external and internal radius for both configurations, it is obtained

$$\frac{1}{2}\left(\frac{r_e}{r_i}\right)^2_{OCE} - \ln\left(\frac{r_e}{r_i}\right)_{OCE} = 1 + \left(\frac{r_e}{r_i}\right)^2_{ICE}\left[\ln\left(\frac{r_e}{r_i}\right)_{ICE} - \frac{1}{2}\right] \quad (11)$$

which allows the comparison of the bed thickness of the three-dimensional structure working with outer or inner counter electrode.

3. Experimental details

The experiments were performed with a cylindrical three-dimensional cathode, 42 mm external diameter, 10 mm internal diameter and 46 mm long. This cathode was made by winding a 316 stainless steel woven-wire mesh, 30 mesh size, (0.25 mm wire diameter and 0.597 mm distance between wires) around a rod. The cathodic geometric surface area was approximately 0.253 m^2, giving a surface area per unit electrode volume of 4208 m^{-1} with a void fraction of 0.7, which were calculated by using the following equations [17]

$$A_s = \frac{4w}{d\delta V} \quad (12)$$

and

$$\varepsilon = 1 - \frac{w}{\delta V} \quad (13)$$

where w is the weight of the electrode, d is the wire diameter and δ is the density of the electrode material. For the outer counter electrode arrangement a stainless steel rood, 9.6 mm diameter, worked as cathodic current feeder and a concentric nickel cylinder, 0.5 mm thick and 46 mm long with an external diameter of 44.6 mm was used as anode. This nickel cylinder was also used as cathodic current feeder for the inner counter electrode configuration and for this case the anode was made by winding a stainless steel mesh plated with nickel. Both electrodes were separated by a woven plastic mesh (0.5 mm thickness, 0.25 mm thread diameter, 0.28 mm distance between threads and 0.81 void fraction) or two layer of a cellulosic sheet (0.18 mm thickness and 90 g m^{-2} grammage) to avoid an electrical contact between them. The electrodes were placed in the central part of an acrylic tube, 44.6 internal diameter and 250 mm long, whose inlet and outlet regions were filled with glass beads of 4 mm diameter in order to ensure a uniform distribution of electrolyte in the reaction region and to reduce channelling effects. The electrical connection of the outer electrode was made by a nickel wire passed through the reactor wall and pressing the nickel plate. The connection to the

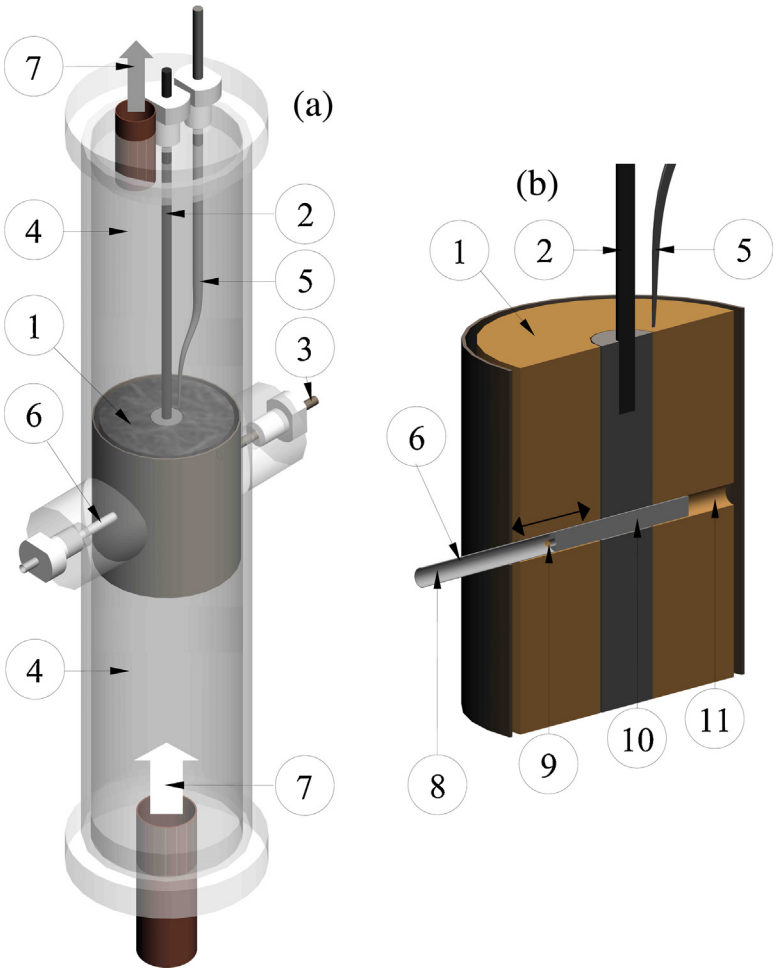

Fig. 2. (a) Schematic representation of the cylindrical electrochemical reactor. (b) View of the Haber-Luggin capillary used to measure the potential distribution. (1) Three-dimensional cathode; (2) electrical connection for the inner electrode; (3) electrical connection for the outer electrode; (4) glass beads; (5) Haber-Luggin capillary to control the cathodic potential; (6) Haber-Luggin capillary to measure the potential distribution; (7) electrolyte flow; (8) connection to reference electrode to measure the potential distribution; (9) lateral hole in the capillary; (10) silicone seal in the capillary; (11) radial hole in the three-dimensional structure.

Table 1
Physicochemical properties of the ferricyanide/ferrocyanide solution.

Composition	$[K_3Fe(CN)_6] = 5 \times 10^{-3}$ mol dm^{-3} $[K_4Fe(CN)_6] = 0.1$ mol dm^{-3} $[K_2CO_3] = 1.75$ mol dm^{-3}
ρ^0/Ω m	5.44×10^{-2}
ν /m^2 s^{-1}	1.52×10^{-6}
D /m^2 s^{-1}	5.3×10^{-10}
Sc	2868

inner electrode was made through the upper part of the reactor. Fig. 2 (a) sketches the experimental arrangement. The reactor was made part of a flow circuit system consisting of a pump, a flow meter and connections to maintain the temperature at the preset value, 30 °C. Thus, the electrolyte and current flows are at right angle, usually called flow-by configuration.

The test reaction was the electrochemical reduction of ferricyanide from solutions with $[K_3Fe(CN)_6] \cong 5 \times 10^{-3}$ mol dm^{-3}, $[K_4Fe(CN)_6] \cong 0.1$ mol dm^{-3}, in 1.75 mol dm^{-3} of K_2CO_3 as supporting electrolyte. Table 1 summarizes the composition and physicochemical properties of the solution, which were measured in the laboratory.

According to the plug flow model under limiting current conditions the concentration at the reactor oulet, c_o, is given by [18]

$$c_o = c_i e^{-\beta} \tag{14}$$

Being c_i the concentration at the reactor inlet and β is a dimensionless number which lumps the global mass-transfer coefficient, k_m, geometric electrode parameters, A_s and V, with the volumetric flow rate, Q, defined as

$$\beta = \frac{k_m A_s V}{Q} \tag{15}$$

Taking into account Eq. (14), β must be less than 0.05 to obtain a concentration change along the reactor lower than 5%. Thus, in order to approach the assumption of constant concentration in the reactor, the reaction at the counter electrode is the reverse than that at the working electrode.

Nitrogen was bubbled in the reservoir for 1 h prior to the experiment in order to remove the dissolved oxygen. A big difference in concentration between ferricyanide and ferrocyanide was chosen in order to achieve the same total current at both

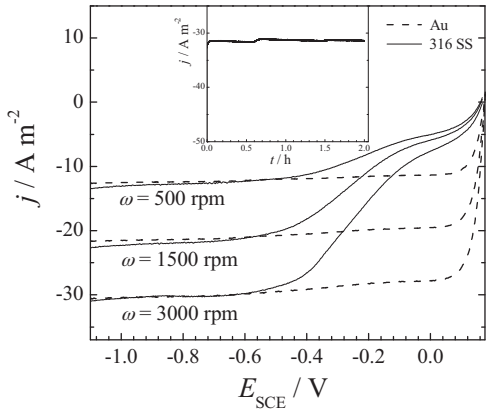

Fig. 3. Polarization curves for the ferricyanide reduction at rotating disc electrodes of gold and 316 stainless steel. $[K_3Fe(CN)_6] \cong 5 \times 10^{-3}$ mol dm^{-3}, $[K_4Fe(CN)_6] \cong 0.1$ mol dm^{-3}, in 1.75 mol dm^{-3} of K_2CO_3 as supporting electrolyte. $T = 30$ °C. Potential sweep rate: 2 mV s^{-1}. Inset: Current as a function of time, $\omega = 3000$ rpm, $E_{SCE} = -0.85$ V.

electrodes, i.e. the three-dimensional cathode and the nickel anode with a smaller surface area, without a secondary reaction at the counter electrode. The high concentration of supporting electrolyte was adopted to diminish the oxygen solubility in the electrolyte [19]. Thus, the current for the reduction of the residual oxygen after bubbling nitrogen is negligible in comparison with the reduction current of ferricyanide from this dilute solution. Samples of the electrolyte were taken from the reservoir after each experiment and the ferricyanide concentration was spectrophotometrically determined at a wavelength of 422 nm, using a Perkin-Elmer model Lambda 20 double-beam UV–vis Spectrophotometer with 10 mm glass absorption cells and the supporting electrolyte was used as blank. The experiments were performed potenciostatically, the cathodic potential was controlled against a saturated calomel electrode, SCE, connected to a Haber-Luggin capillary positioned at the inner radius of the cathode. The potential distribution was measured by using a second saturated calomel electrode with a capillary, which was displaced along the thickness of the cylindrical three-dimensional cathode. Fig. 2(b) shows schematically the assembly for the measurement of the potential distribution. Thus, a capillary tube was introduced in a radial hole through the arrangement of both electrodes. The tube presents a lateral hole to measure the potential distribution in radial direction between the inner and outer radius of the cathode. The final part of the tube was sealed with silicone and it fully fills the hole in the cathode between the internal and external radius in order to hinder the flow of current through it, which could alter the potential distribution in the electrode.

4. Results and discussion

4.1. Experiments with a rotating disc electrode

Prior to the potential distribution measurements, the electrochemical behaviour of the test reaction was studied at rotating disc electrodes, 3 mm diameter, of gold and 316 stainless steel. Fig. 3 shows a set of polarization curves, where in all cases a well defined limiting current density can be observed and the results for both metals coincide at potentials more negative than −0.6 V, where a limiting current density is achieved. The different behaviour at potentials higher than −0.6 V can be attributed to the corrosion of 316 stainless steel. The current as a function of time for the reduction of ferricyanide at a 316 stainless steel rotating disc electrode is given in the inset of Fig. 3, where it is observed a constant current density during a long time. Then, 316 stainless steel can be recognized as an appropriate material to make the three-dimensional electrode, which allows as test reaction the ferricyanide reduction with K_2CO_3 as supporting electrolyte. Thus, limiting current conditions are obtained in a wide range of potentials for values more negative than −0.6 V against SCE.

4.2. Experiments with the cylindrical three-dimensional electrode.

Figs. 4 and 5 report the local electrode potential as a function of the radial position inside the three-dimensional structure at different Reynolds numbers for the arrangements with outer or inner counter electrode, respectively. Each point represents the mean value of three-independent experiments and the segments correspond to its standard deviation. The theoretical behaviour given by Eq. (9) is represented as full lines. A close agreement between the theoretical and experimental potential distributions can be observed in both figures. Fig. 6 shows the potential difference evaluated at the external and internal radius divided by the product between the current and the effective resistivity of the electrolyte as a function of the Reynolds number. The full lines represent the theoretical behaviour according to Eq. (10), where is

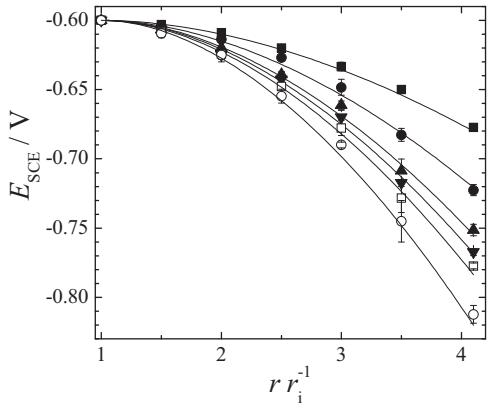

Fig. 4. Distribution of the electrode potential as a function of the radial position, *r*, at different Reynolds numbers. Outer counter electrode arrangement. r_i is the internal radius of the three-dimensional electrode. $T = 30\,^{\circ}C$. (■): Re = 0.789, $I = 0.657$ A. (●): Re = 1.421, $I = 0.993$ A. (▲): Re = 2.089, $I = 1.273$ A. (▼): Re = 2.795, $I = 1.383$ A. (□): Re = 3.537, $I = 1.510$ A. (○): Re = 4.318, $I = 1.810$ A. Full lines: theoretical behaviour according to Eq. (9). Segments: standard deviation.

corroborated a close agreement between the experimental and theoretical results. From Figs. 4–6, it is detected that the arrangement with inner counter electrode presents a higher potential distribution than the configuration with outer counter electrode. Then, this configuration shows the best performance for a given value of current.

Fig. 7 shows the bed thickness for both configurations, inner and outer counter electrode, under constant operating conditions for the same value of the potential difference between the inner and outer radius. The calculations were performed according to Eq. (11). Fig. 7 corroborates the best performance of the arrangement with outer counter electrode [16], which shows the largest bed thickness and consequently, under limiting current conditions, a higher current that increases the fractional conversion per pass.

4.3. Mass-transfer results.

The global mass-transfer coefficient was calculated from the limiting current, I_L, recorded at different flow rates and by using the expression

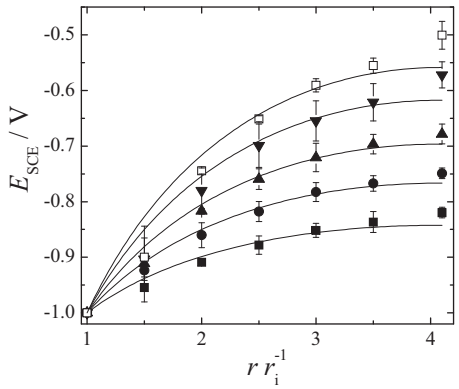

Fig. 5. Distribution of the electrode potential as a function of the radial position, *r*, at different Reynolds numbers. Inner counter electrode arrangement. r_i is the internal radius of the three-dimensional electrode. $T = 30\,^{\circ}C$. (■): Re = 0.751, $I = 0.500$ A. (●): Re = 1.351, $I = 0.740$ A. (▲): Re = 1.987, $I = 0.963$ A. (▼): Re = 2.658, $I = 1.213$ A. (□): Re = 3.364, $I = 1.400$ A. Full lines: theoretical behaviour according to Eq. (9). Segments: standard deviation.

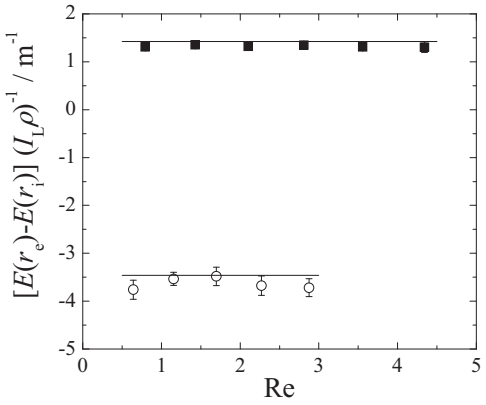

Fig. 6. Potential difference evaluated at the external and internal radius divided by the product between the current and the effective resistivity of the electrolyte as a function of the Reynolds number. Full lines: theoretical behaviour according to Eq. (10).

$$k_m = -\frac{Q}{A_s V}\ln\left(1 - \frac{I_L}{\nu_e F Q c_i}\right) \tag{16}$$

Eq. (16) assumes that the electrochemical reactor can be represented by the plug flow model and that the current efficiency is 100%. To compare the present experiments with previous correlations for three-dimensional electrodes made of woven-wire meshes, the j_d factor for mass-transfer given by [20]

$$j_d = \frac{k_m}{u/\varepsilon} Sc^{2/3} \tag{17}$$

is reported in Fig. 8 as a function of the Reynolds number. Here, *u* is the superficial electrolyte flow velocity. The Reynolds and Schmidt numbers are defined as

$$Re = \frac{ud}{\varepsilon\nu} \tag{18}$$

and

$$Sc = \frac{\nu}{D} \tag{19}$$

being *d* the wire diameter, *D* the diffusion coefficient and ν the kinematic viscosity. It can be observed that the results agree well with the extrapolation of the equation given by Storck et al. [21], Eq. (20), which was also determined for a stack of nets arranged

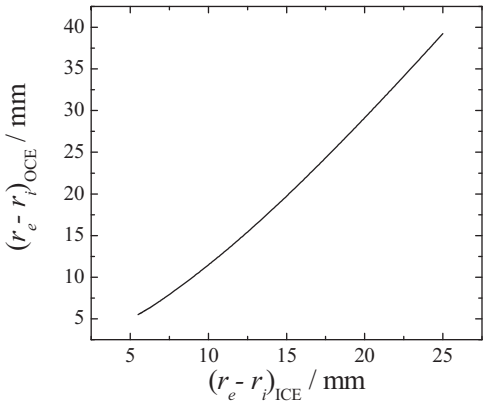

Fig. 7. Bed thickness of a cylindrical electrochemical reactor with outer counter-electrode in comparison with the bed thickness of an arrangement with inner counterelectrode under constant operating conditions and for the same potential difference between the inner and outer radius. $r_i = 5$ mm.

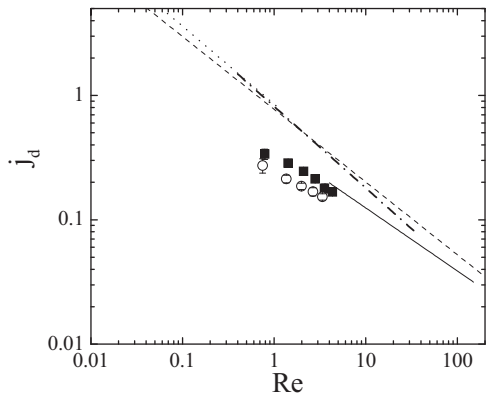

Fig. 8. Comparison of mass-transfer correlations against Reynolds mumber for woven-wire meshes. (■): outer counter electrode arrangement. (○): inner counter electrode arrangement. Segments: standard deviation. Full line: Storck et al. [21]. Dashed line: Vogtländer and Parker [23]. Dotted line: Sioda [24]. Dashed-dotted line: Cano and Böhm [25].

parallel to the electrolyte flow direction with electrolyte and current flows at right angle.

$$j_d = 0.40Re^{-0.507} \quad (20)$$

5. Application of the reactor to copper removal from a dilute solution.

5.1. Experimental details and results.

Deposition of copper from a dilute solution was used as test reaction to determine the behaviour of the electrochemical reactor above described with an outer counter electrode arrangement. The cathode was a cylinder made by winding a 316 stainless steel woven-wire mesh, 30 mesh size, around a copper rod, 13 mm diameter, which worked as cathodic current feeder. The cathodic geometric surface area per unit electrode volume was approximately 4685 m^{-1} with a void fraction of 0.71. The external diameter of the cathode was 34 mm and 50 mm long. To maintain constant the copper concentration in the bulk solution a concentric copper cylinder, 1 mm thick and 50 mm long with an internal diameter of 40 mm was used as anode. The electrodes were separated by two layer of the woven plastic mesh above described.

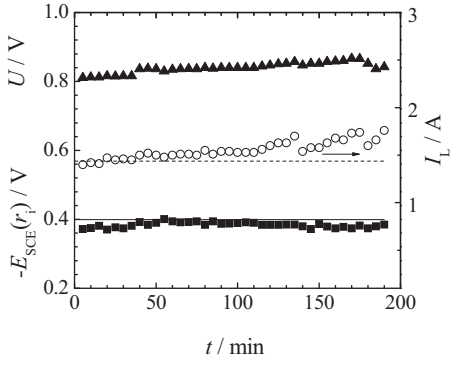

Fig. 9. Electrical parameters for the copper deposition in a cylindrical electrochemical reactor with a three-dimensional cathode composed by woven-wire meshes. Outer counter electrode arrangement. Potentiostatic control with $E_{SCE}(r_e) = -0.65$ V. $Q = 4.37 \times 10^{-6}$ m^3 s^{-1}. $[Cu^{+2}] = 350$ ppm. $T = 30$ °C. Supporting electrolyte: 1 M Na_2SO_4 at pH 2. (■): $E_{SCE}(r_i)$, (○): I_L and (▲): cell voltage, U. Full and dashed lines: theoretical results for $E_{SCE}(r_i)$, and I_L, respectively.

Table 2
Physicochemical properties of the copper sulphate electrolyte.

Composition	$[Cu^{+2}] \cong 350$ ppm in 1 M Na_2SO_4 at pH 2
ρ^0/Ω m	9.72×10^{-2}
$\nu/m^2 s^{-1}$	1.11×10^{-6}
$D/m^2 s^{-1}$	5.1×10^{-10}
Sc	2176

The experiments were performed potentiostatically, two saturated calomel electrodes were used as reference electrodes, each being connected to Haber-Luggin capillaries. One of them was positioned in the side of the cathode nearest to the counter electrode, which represents the most negative potential of the stack and was controlled by the potentiostat at −0.65 V against SCE in order to hamper the hydrogen evolution [17]; while the second one was positioned in the side of the cathode farthest from the anode. This reference electrode measures the less negative potential of the three-dimensional cathode, which was also recorded during the experiment. The difference between the potentials of the reference electrodes gives the ohmic drop in the solution phase inside the stack of nets.

The electrolyte solution was 1 M Na_2SO_4 and H_2SO_4, to obtain pH 2, with a copper concentration of approximately 350 ppm.

Fig. 9 shows the cathode potential at the side farthest from the counter electrode, the cell voltage and the current as a function of time. The full and dashed lines in Fig. 9 represent the theoretical values of $E_{SCE}(r_i)$ and total current, which were calculated with Eq. (9) and Eq. (2), respectively. For these calculations were used the physicochemical parameters reported in Table 2 and Eq. (20) for the evaluation of the mass-transfer coefficient. The error between the mean values of the experimental results and the theoretical ones was 4% for the cathode potential at r_i and 7.5% for the total current. Thus, within the accuracy expected for this type of experiments it is detected a close agreement between the experimental and theoretical results, which validates the mathematical treatment for the removal of metals from dilute solutions. The final void fraction was 0.69, its small change during the experiment corroborates the first assumption of the model. However, the increase of the experimental current with time, showed in Fig. 9, can be explained taking into account the change of the surface area due to the metal deposition, which becomes more important in prolonged experiments making unpredictable the behaviour of the electrochemical reactor.

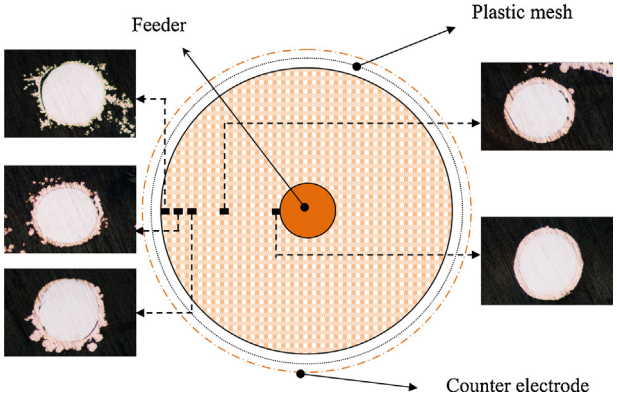

Fig. 10. Morphology of the deposits as a function of its position in the three-dimensional cathode. Outer counterelectrode arrangement. Potentiostatic control with $E_{SCE}(r_e) = -0.65$ V. $Q = 4.37 \times 10^{-6}$ m^3 s^{-1}. $[Cu^{+2}] = 350$ ppm. Supporting electrolyte: 1 M Na_2SO_4 at pH 2. $T = 30$ °C. $t = 16$ h. Magnification × 100.

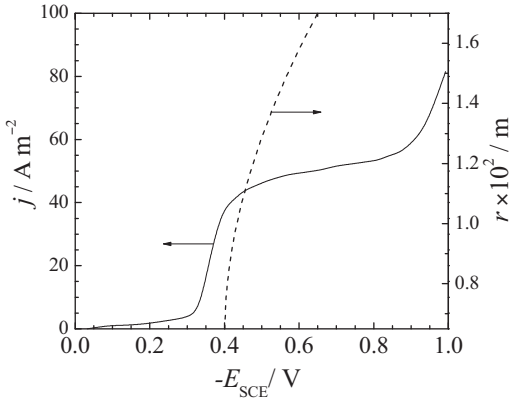

Fig. 11. Polarization curve for copper deposition obtained with a rotating disc electrode. $T = 30\,^{\circ}C$. Rotation speed = 1012 rpm. $[Cu^{+2}] = 352$ ppm. Supporting electrolyte: 1 M Na_2SO_4 at pH 2. Dashed line: theoretical potential as a function of the position inside the bed, according to Eq. (9).

5.2. Morphological characterization of the electrodeposited copper

At the end of the experiment, 16 h, an epoxy resin was poured into the three-dimensional cathode and cured. Cross-sections of the cathode were polished and examined with a metallurgical microscope in order to observe the morphological characteristics of the electrodeposits and to examine the thickness distribution of the deposits along the electrode thickness. Thus, Fig. 10 reports some micrographs of cross-sections of wires, magnification ×100, as a function of their position in the three-dimensional cathode. The deposits obtained in the zones near the counter electrode show dendritic characteristics and those electrodeposited in the region from the central part to the current feeder are nodular, where less negative values of potential are achieved. Fig. 11 shows a typical polarization curve for copper deposition obtained with a rotating disc electrode and the dashed line represents the theoretical variation of the potential inside the cathode according to Eq. (9). It can be appreciated an important variation of the potential along the bed thickness, which produces that the copper deposition presents changing morphologies. Thus, the electrode regions at more cathodic potentials show a dendritic nature and nodular deposits take place at the less cathodic areas. Likewise, the presence of the separator near the counter electrode can modify the hydrodynamics altering the characteristics of the electrodeposits.

Furthermore, Fig. 10 also reports that for a given radial position in the bed the thickness of the deposit is generally similar in all the perimeter of the wire. However, some abnormal situations were observed. Thus, Fig. 12, Part (a) shows a micrograph of the intersection between two wires; where, due to the shielding effect, the thickness of the deposit is lower in the contact region of the wires. Likewise, Part (b) in Fig. 12 reports a portion of a wire with a dendritic formation in a region near the current feeder, where a nodular deposit is expected. This astonishing behaviour may be attributed to the lack of uniformity in the hydrodynamics inside the bed. Thus, it is possible a by-pass of electrolyte in an electrode region and the generation of a stagnant zone in the neighbourhood, where the decrease in concentration increases the mass-transfer control inducing the dendritic growing. Fig. 12, part (a) and (b), gives additional experimental evidence that the surface electrode area of a three-dimensional electrode is not equally accessible [17,22].

Fig. 12 part (c) shows a SEM micrograph of the copper detached from the three-dimensional cathode, magnification ×1500. As expected all morphologies are present in the final product, which defines the applications of the copper powders obtained by electrolysis from dilute solutions with three-dimensional electrodes. It must be emphasized that the morphological characteristics, above reported, were also observed in additional experiments performed with electrochemical reactors of flow-by or flow-through configuration.

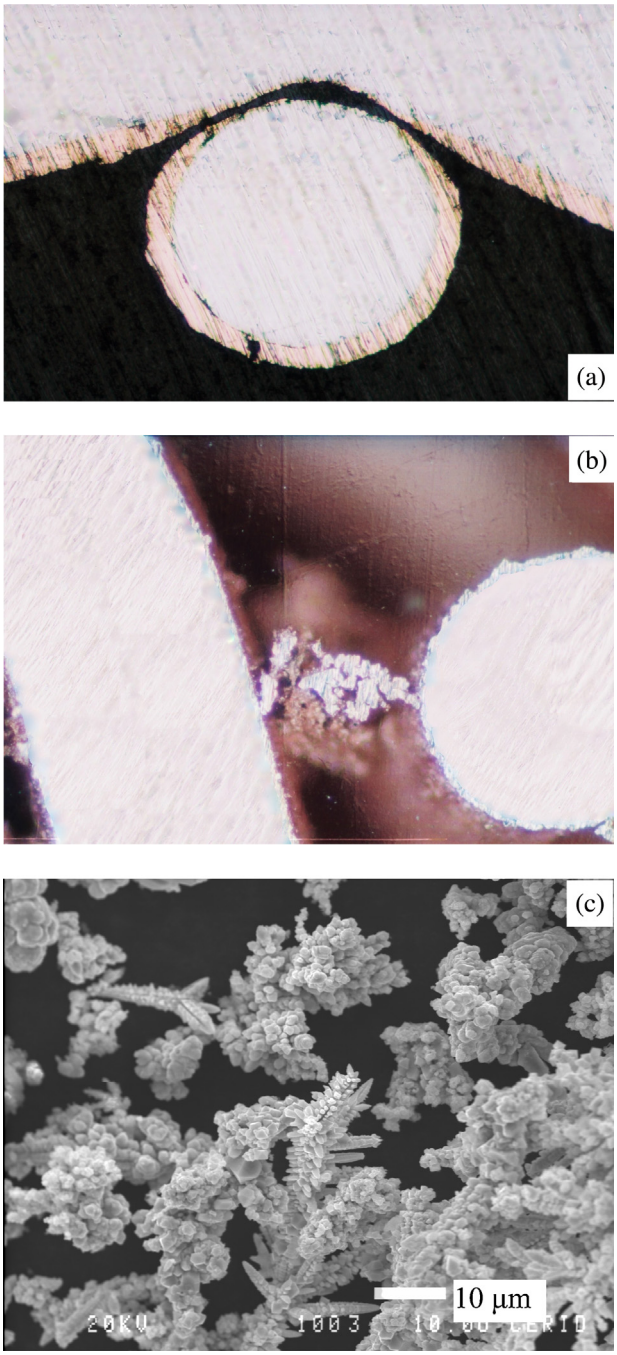

Fig. 12. Abnormal deposits and powder morphology. Part (a): Shielding effect in the intersection of two wires. Magnification × 100. Part (b): Dendritic deposit in a zone of low potential. Magnification × 100. (c): Scanning electron micrograph of copper powder detached from the three-dimensional cathode. Magnification: ×1500.

6. Conclusions

The following conclusions may be drawn:

(i) A mathematical treatment based on the continuous model of three-dimensional electrodes is appropriate to predict the

behaviour of a cylindrical electrochemical reactor with a flow-by configuration.

(ii) The arrangement with an outer counter electrode presents the best performance, because it drains more current with the same potential difference in the three-dimensional electrode.

(iii) In a three-dimensional cathode the morphology of the deposit varies with the position because of the potential distribution in the electrode and changes in the hydrodynamic conditions.

(iv) In general, the deposit thickness is uniform for a given radial position in the bed. Exceptions are detected as a consequence of the shielding between wires or hydrodynamic irregularities.

Acknowledgements

This work was supported by the Agencia Nacional de Promoción Científica y Tecnológica (ANPCyT), Consejo Nacional de Investigaciones Científicas y Técnicas (CONICET) and Universidad Nacional del Litoral (UNL) of Argentina.

References

[1] L.M. Abrantes, Three-dimensional electrode, in: G. Kreysa, K.-i. Ota, R.F. Savinell (Eds.), Encyclopedia of Applied Electrochemistry, Springer, New York, 2014, pp. 2077.
[2] L.L. Bott, How Nalco makes lead akyks, Hydrocarbon Processing 44 (1965) 115.
[3] G. van der Heiden, C.M.S. Raats, H.F. Boon, Fluidized bed electrolysis for removal or recovery of metals from dilute solutions, Chemistry and Industry (London) 13 (1978) 465.
[4] G. van der Heiden, C.M.S. Raats, H.F. Boon, Eine Wirbelbettelektrolysezelle zur Entfernung von Metallen aus Abwasser, Chemie Ingenieur Technik 51 (1979) 651.
[5] C.H. Elges III, M.D. Wrobleswski, J.A. Eisele, Direct electrowinning of gold, in: P. E. Richardson, S. Srinivasan, R. Woods (Eds.), Proceedings of the International Symposium on Electrochemistry in Mineral and Metal Processing, The Electrochemical Society, Pennington N. J, 1984, pp. 501.
[6] G. Kreysa, Elektrochemie mit dreidimensionalen Elektroden, Chemie Ingenieur Technik 55 (1983) 23.
[7] K. Bouzek, R. Chmelíková, M. Paidar, H. Bergmann, Study of mass transfer in a vertically moving particle bed electrode, Journal of Applied Electrochemistry 33 (2003) 205.
[8] K. Bouzek, H. Bergmann, Mathematical simulation of a vertically moving particle bed electrochemical cell, Journal of Applied Electrochemistry 33 (2003) 839.
[9] G.W. Reade, C. Ponce de León, F.C. Walsh, Enhanced mass transport to a reticulated vitreous carbon rotating cylinder electrode using jet flow, Electrochimica Acta 51 (2006) 2728.
[10] J.M. Grau, J.M. Bisang, Mass transfer studies at rotating cylinder electrodes of expanded metal, Journal of Applied Electrochemistry 35 (2005) 285.
[11] J.M. Grau, J.M. Bisang, Mass transfer studies at packed bed rotating cylinder electrodes of woven-wire meshes, Journal of Applied Electrochemistry 36 (2006) 759.
[12] J.M. Grau, J.M. Bisang, Electrochemical removal of cadmium from dilute aqueous solutions using a rotating cylinder electrode of wedge wire screens, Journal of Applied Electrochemistry 37 (2007) 275.
[13] O. González Pérez, J.M. Bisang, Electrochemical synthesis of hydrogen peroxide with a three-dimensional rotating cylinder electrode, Journal of Chemical Technology and Biotechnology 89 (2014) 528.
[14] R. Alkire, P.K. Ng, Two-dimensional current distribution within a packed-bed electrochemical flow reactor, Journal of the Electrochemical Society 121 (1974) 95.
[15] R. Alkire, P.K. Ng, Studies on flow-by electrodes having perpendicular directions of current and electrolyte flow, Journal of the Electrochemical Society 124 (1977) 1220.
[16] G. Kreysa, K. Jüttner, J.M. Bisang, Cylindrical three-dimensional electrodes under limiting current conditions, Journal of Applied Electrochemistry 23 (1993) 707.
[17] J.M. Bisang, Theoretical and experimental studies of the effect of side reactions in copper deposition from dilute solutions on packed-bed electrodes, Journal of Applied Electrochemistry 26 (1996) 135.
[18] D.J. Pickett, Electrochemical Reactor Design, 2nd ed, ELSEVIER, Amsterdam, 1979.
[19] R. Battino, T.R. Rettich, T. Tominaga, The solubility of oxygen and ozone in liquids, Journal of Physical and Chemical Reference Data 12 (1983) 163.
[20] N. Ibl, O. Dossenbach, Convective mass transport, in: E. Yeager, J.O.M. Bockris, B.E. Conway (Eds.), Comprehensive Treatise of Electrochemistry, Plenum Press, New York, 1983, pp. 133.
[21] A. Storck, P.M. Robertson, N. Ibl, Mass transfer study of three-dimensional electrodes composed of stacks of nets, Electrochimica Acta 24 (1979) 373.
[22] R. Alkire, B. Gracon, Flow-through porous electrodes, Journal of the Electrochemical Society 122 (1975) 1594.
[23] P.H. Vogtländer, C.A.P. Bakker, An experimental study of mass transfer from a liquid flow to wires and gauzes, Chemical Engineering Science 18 (1963) 583.
[24] R.E. Sioda, Mass transfer problems in electrolysis with flowing solution on single and stacked screens, Journal of Electroanalytical Chemistry 70 (1976) 49.
[25] J. Cano, U. Böhm, Mass transfer in packed beds of screens, Chemical Engineering Science 32 (1977) 213.